EFFECTS OF Mg, Si AND Cu ON AGEING RESPONSE OF DILUTE 6XXX SERIES ALUMINIUM ALLOYS

by

CHE NOR AIZA BINTI JAAFAR

**Thesis submitted in fulfilment
of the requirements for the degree of
Doctor of Philosophy**

February 2011

ACKNOWLEDGEMENTS

The author wishes to express her sincere thanks and appreciation to Assoc. Prof. Dr. Azmi Rahmat of Universiti Sains Malaysia (USM) for his valuable help and guidance throughout this research work. Thanks are also to Dr. Zuhailawati Hussain for being my co-supervisor.

I would like to thank to Dr. Mat Hussain, En. Ahmad Damanhuri, En Zubir, En Zaini, Pn Banjuraizah, Mr. Peter Kenway, Mr. Michael Faucker and Mr. Stephen for their support during my research work.

Special thanks are to Assoc. Prof Dr. Ismail Zainol, Dr. Mohd Harun, Dr. Ian Davidson, Dr. Pete Apps and Dr. Mallike for valuable help and support.

Thanks are also to all my friends especially to Dayang Habibah, Dr. Roslinda, Dr. Faieza, Dr. Megat, Tn Hj Yunin, Prof. Dr. Shamsuddin, Prof. Dr. Safuan, Jun Aida, Nor Aida, Kak Linda and Kak Ros during the course of this project.

Finally, I would like to express my gratitude to my beloved husband, my parents and all of my family for their prayer, encouragement and support throughout my thesis.

TABLE OF CONTENTS

		Page
ACKNOWLEDGEMENTS		ii
TABLE OF CONTENTS		iii
LIST OF TABLES		ix
LIST OF FIGURES		xi
LIST OF SYMBOLS		xxi
LIST OF ABBREVIATIONS		xxiv
ABSTRAK		xxv
ABSTRACT		xxvi
CHAPTER 1: INTRODUCTION		
1.1	Aluminium and Its Alloys	1
1.2	Problem Statement	4
1.3	Objectives of the Project	5
1.4	Organisation of the Thesis	6
CHAPTER 2: LITERATURE REVIEW		
2.1	Heat Treatment	8
	2.1.1 Solution Treatment	10
	2.1.2 Quenching	10
	2.1.3 Ageing	11
2.2	Strengthening in Aluminium Alloys	15
	2.2.1 Mechanical Properties of Aluminium Alloys	15
	2.2.1.1 Intermetallic Compounds	15
	2.2.1.2 Dispersoids	17
	2.2.1.3 Fine Precipitates	19
	2.2.2 Strengthening Mechanisms	19
	2.2.2.1 Work Hardening (Strain Hardening)	19
	2.2.2.2 Grain Size Strengthening	20
	2.2.2.3 Solid Solution Strengthening	21

2.2.2.4 Particle Hardening 22
2.2.3 The Effect of Precipitates on the Strength of Alloys 22
2.3 Precipitation Hardening 25
2.3.1 Precipitation and Matrix Interfaces 26
2.3.2 Thermodynamics of Precipitation Reaction from Solid Solution 27
2.3.2.1 Precipitate Nucleation 27
2.3.3 The Formation of Transition Phases 34
2.3.4 Precipitate Growth from Supersaturated Solid Solution 35
2.3.5 Precipitate Coarsening 35
2.3.6 The Effect of Trace Elements 37
2.4 Overview of the 6xxx Series Alloys 38
2.4.1 Commercial 6xxx Series Alloys 40
2.4.1.1 Balanced Al-Mg_2Si Alloys 40
2.4.1.2 Intermediate Al-Mg_2Si Alloys 41
2.4.1.3 Excess Si Al-Mg_2Si Alloys 41
2.4.2 Element Additions to 6xxx Series Alloys 43
2.4.2.1 Copper 43
2.4.2.2 Manganese, Chromium and Zirconium 45
2.4.2.3 Other Elements 46
2.4.3 Application of 6xxx Series Alloys in Automotive Industry 48
2.4.4 Precipitation Sequences of 6xxx Series Alloys 51
2.5 The Extrapolation Technique 58

CHAPTER 3: EXPERIMENTAL

3.1 Materials 60
3.2 JMatPro Calculations 61
3.3 Differential Scanning Calorimetry (DSC) 62
3.4 Ageing Treatments 63
3.5 Characterisation of Microstructure 64
3.5.1 Optical Microscopy 64
3.5.2 Polarized Light Optical Microscopy 65

3.5.3 Transmission Electron Microscopy (TEM) 66
3.5.4 Thickness and Density Measurement 67
3.5.5 SEM-EDX (Energy Dispersive X-ray Microanalysis) 67
3.5.6 TEM-EDX (Energy Dispersive X-ray Microanalysis) 68
3.6 Image Analyses 68
3.7 Mechanical Testing 69
3.7.1 Vickers Hardness Testing 69
3.7.2 Tensile Testing 70

CHAPTER 4: RESULTS

4.1 JMatPro Calculations 71
4.1.1 Cu-containing Alloys 71
4.1.2 Cu-free Alloys 74
4.2 As-Received Alloys 78
4.2.1 Optical Microscopy of As-Received Alloys 78
4.2.2 SEM-EDX of As-Received Alloys 84
4.2.3 Image Analysis of As-Received Alloys 87
4.2.4 Polarized Light Optical Microscopy of As-Received Alloys 88
4.3 Solution Treated Alloys 96
4.3.1 Optical Microscopy of Solution Treated Alloys 96
4.3.2 SEM-EDX of Solution Treated Alloys 102
4.3.3 TEM-EDX of Solution Treated Alloys 104
4.3.4 Image Analysis of Solution Treated Alloys 117
4.3.5 Polarized Light Optical Microscopy of Solution Treated Alloys 118
4.3.6 Differential Scanning Calorimetry (DSC) 126
4.4 Naturally Aged Alloys 131
4.4.1 Natural Ageing Responses of Cu-containing and Cu-free Alloys 131
4.4.1.1 Natural Ageing Responses of Cu-containing Alloys 132
4.4.1.2 Natural Ageing Responses of Cu-free Alloys 132
4.4.2 Tensile Strength of Naturally Aged Alloys 133

4.4.2.1 Tensile strength of Naturally Aged Cu-containing Alloys 134
4.4.2.2 Tensile strength of Naturally Aged Cu-free Alloys 136
4.4.2.3 The Effect of Composition on Tensile Strength of Naturally Aged Alloys 138
4.5 Artificially Aged Alloys 142
4.5.1 Artificial Ageing Responses of Cu-containing and Cu-free Alloys 142
4.5.1.1 Ageing Response of Artificially Aged Cu-containing Alloys 144
4.5.1.2 Ageing Response of Artificially Aged Cu-free Alloys 146
4.5.1.3 The Effect of Ageing Time and Temperature on Hardness 149
4.5.1.4 Summary of Artificially Aged Alloys Results 154
4.5.2 Tensile Strength of Artificially Aged Alloys 156
4.5.2.1 Tensile Strength of Artificially Aged Cu-containing Alloys 157
4.5.2.2 Tensile Strength of Artificially Aged Cu-free Alloys 159
4.5.2.3 The Effect of Composition on Tensile Strength of Artificially Aged Alloys 163
4.5.2.4 The Effect of Ageing Temperature on the Tensile Properties of Cu-containing and Cu-free Alloys 165
4.5.3 Transmission Electron Microscopy (TEM) 169
4.5.3.1 Density and Length of Precipitates Measurement 176
4.5.3.2 Precipitates Identification 178

CHAPTER 5: DISCUSSION

5.1 JMatPro Calculations 182
5.2 As-Received Alloys 183
5.2.1 Optical Microscopy of As-Received Alloys 183
5.2.2 SEM-EDX of As-Received Alloys 183
5.2.3 Image Analyses of As-Received Alloys 184
5.2.4 Polarized Light Optical Microscopy of As-Received Alloys 185
5.3 Solution Treated Alloys 185
5.3.1 Optical Microscopy of Solution Treated Alloys 185

5.3.2 SEM-EDX of Solution Treated Alloys 186
5.3.3 TEM-EDX of Solution Treated Alloys 187
5.3.4 Image Analysis of Solution Treated Alloys 189
5.3.5 Polarized Light Optical Microscopy of Solution Treated Alloys 190
5.4 Ageing Responses 191
5.4.1 Differential Scanning Calorimetry (DSC) 191
5.4.2 Hardness Measurements 194
5.4.2.1 Effect of Composition on the Natural Ageing Behaviour 194
5.4.2.2 Effect of Composition on the Artificial Ageing Behaviour 196
5.4.2.3 The Effect of Ageing Time and Temperature on Hardness 198
5.4.3 Tensile Properties 201
5.4.3.1 Effect of Composition on Tensile Properties of Naturally Aged Alloys 201
5.4.3.2 Effect of Composition on Tensile Properties of Artificially Aged Alloys 202
5.4.4 The Effect of Composition on the Microstructure of Aged Alloys 204
5.4.4.1 Ageing for 1000 hours at 100 ^{o}C 204
5.4.4.2 Ageing for 30 hours at 185 ^{o}C 205
5.4.4.3 Ageing at 300 ^{o}C 207
5.5 Summary 212

CHAPTER 6: CONCLUSIONS AND FUTURE WORK

6.1 Conclusions 217
6.2 Future Work 219

REFERENCES 220

APPENDICES
Appendix A Calculation of Mg_2Si and ExSi contents 231
Appendix B Using Convergent Beam Electron Diffraction (CBED) method to determine the thickness of thin foil 232

Appendix C	Determination of density of precipitates	234
Appendix D	Raw data of TEM-EDX (extrapolation technique)	235
Appendix E	Heat treatment hardness data	240
Appendix F	Tensile Test data	244
Appendix G	Possible chemical formula of the coarse precipitates labelled as P, Q, R and S (alloy B4 after ageing at 300 ^{o}C for 1000 hours)	251
Appendix H	List of publications	252

LIST OF TABLES

		Page
Table 2.1	Compositions (wt %) of selected 6xxx series alloys	39
Table 2.2	Mechanical properties of selected 6xxx series alloys	40
Table 2.3	Typical applications of selected 6xxx series in the automotive industry	50
Table 3.1	Chemical composition of the Cu-containing alloys (wt %)	61
Table 3.2	Chemical composition of the Cu-free alloys (wt %)	61
Table 3.3	Samples of artificially aged alloys with a specific temperature and time of ageing.	67
Table 4.1	Summary of JMatPro calculations results	77
Table 4.2	Image analyses results of the as-received Cu-containing alloys	87
Table 4.3	Image analyses results of the as-received Cu-free alloys	87
Table 4.4	Grain size measurements of as-received Cu-containing alloys	88
Table 4.5	Grain size measurements of as-received Cu-free alloys	88
Table 4.6	TEM-EDX analyses, shape and dimensions of the particles (labelled as A and B) of Cu-containing and Cu-free alloys following solution treatment at 530 ^{o}C for 5 minutes	110
Table 4.7	Possible chemical formula of the selected particles labelled as A and B obtained from different Cu-containing and Cu-free alloys using EDX data analysis	111
Table 4.8	Image analyses results of the solution treated Cu-containing alloys	117
Table 4.9	Image analyses results of the solution treated Cu-free alloys	117
Table 4.10	Grain size measurements of the solution treated Cu-containing alloys	118
Table 4.11	Grain size measurements of the solution treated Cu-free alloys	118
Table 4.12	Time to reach peak hardness and peak hardness values at ageing between 100 ^{o}C to 300 ^{o}C for Cu-containing alloys	155
Table 4.13	Time to reach peak hardness and peak hardness values at ageing between 100 ^{o}C to 300 ^{o}C for Cu-free alloys	156
Table 4.14	The number density and average length of the needle-shaped precipitates after ageing at 185 ^{o}C for 30 minutes	178

Table 4.15 The number density and average length of the needle or rod-shaped precipitates after ageing at 300 C for 3 min (UA), 1 hour (close to PA) and 1000 hours (OA) 178

LIST OF FIGURES

		Page
Figure 1.1	The markets of aluminium consumption in United State and China in the year 2002.	2
Figure 2.1	The pseudo-binary Al and Mg_2Si phase diagram.	9
Figure 2.2	Natural and artificial ageing response.	11
Figure 2.3	Cutting of a fine precipitate by a dislocation.	23
Figure 2.4	Schematic representation of interaction of dislocation with particles (Orowan looping).	24
Figure 2.5	Schematic representation of relationship between strength and precipitate particles size for a typical age-hardening alloys: (A) particles sheared or cut by dislocations: (B) particles passed or bowed by dislocation.	25
Figure 2.6	Interphase boundries in solids (a) Coherent interface (b) Semi-coherent interface and (c) Incoherent interface.	26
Figure 2.7	The variation of free energy with spherical precipitate radius for a homogeneous nucleus.	29
Figure 2.8	The critical nucleus size for grain boundary nucleation	31
Figure 2.9	Critical nucleus shape for nucleation on grain edge.	32
Figure 2.10	Critical nucleus shapes for nucleation on grain corner.	32
Figure 2.11	A schematic molar free energy diagram for the aluminium-X system.	34
Figure 2.12	The origin of particle coarsening β with small radius of curvature (r_2) has a higher molar free energy than β with a large radius of curvature (r_1). The concentration of solute is therefore highest outside the smallest particles.	36
Figure 2.13	Application of aluminium in passenger car.	50
Figure 2.14	DSC trace of an as-quenched sample of alloy 6022.	55
Figure 2.15	Schematic diagram of possible electron paths in a thin sample containing second phase particles (shown hashed).	59
Figure 2.16	Schematic diagram of the analytical data obtained from the sample shown in Figure 2.15.	59
Figure 3.1	Schematic diagram of DSC cell.	63
Figure 3.2	Schematic diagram of the heat treatment cycle of the specimens.	64

Figure 3.3	The top, longitudinal and transverse sections of the extruded alloys.	65
Figure 3.4	Area of indentation.	69
Figure 3.5	Geometry and dimensions of the tensile testing sample.	70
Figure 4.1a	JMatPro calculation shows an equilibrium prediction of the relative amounts of different phases in alloy A1 at different temperature.	72
Figure 4.1b	JMatPro calculation shows an equilibrium prediction of the relative amounts of different phases in alloy A2 at different temperature.	72
Figure 4.1c	JMatPro calculation shows an equilibrium prediction of the relative amounts of different phases in alloy A3 at different temperature.	73
Figure 4.1d	JMatPro calculation shows an equilibrium prediction of the relative amounts of different phases in alloy A4 at different temperature.	73
Figure 4.2a	JMatPro calculation shows an equilibrium prediction of the relative amounts of different phases in alloy B1 at different temperature.	74
Figure 4.2b	JMatPro calculation shows an equilibrium prediction of the relative amounts of different phases in alloy B2 at different temperature.	75
Figure 4.2c	JMatPro calculation shows an equilibrium prediction of the relative amounts of different phases in alloy B3 at different temperature.	75
Figure 4.2d	JMatPro calculation shows an equilibrium prediction of the relative amounts of different phases in alloy B4 at different temperature.	76
Figure 4.2e	JMatPro calculation shows an equilibrium prediction of the relative amounts of different phases in alloy B5 at different temperature.	76
Figure 4.3a	Optical micrographs of the as-received Cu-containing alloys. The pictures were taken of the top section of the alloys. (a) unetched and (b) etched alloys.	79
Figure 4.3b	Optical micrographs of the as-received Cu-free alloys. The pictures were taken of the top section of the alloys. (a) unetched and (b) etched alloys.	80
Figure 4.3b	Continued.	81

Figure 4.4a	Optical micrographs of the as-received Cu-containing alloys. The pictures were taken of the longitudinal section of the alloys. (a) unetched and (b) etched alloys.	82
Figure 4.4b	Optical micrographs of the as-received Cu-free alloys. The pictures were taken of the longitudinal section of the alloys. (a) unetched and (b) etched alloys.	82
Figure 4.5a	Optical micrographs of the as-received Cu-containing alloys. The pictures were taken of the transverse section of the alloys. (a) unetched and (b) etched alloys.	83
Figure 4.5b	Optical micrographs of the as-received Cu-free alloys. The pictures were taken of the transverse section of the alloys. (a) unetched and (b) etched alloys.	83
Figure 4.6	(a) SEM micrographs showing particle labelled as A in alloy A4 and (b) EDX analysis of particle A.	84
Figure 4.7	(a) SEM micrographs showing particle labelled as B in alloy A4 and (b) EDX analysis of particle B.	85
Figure 4.8	(a) SEM micrographs showing particle labelled as C in alloy B4 and (b) EDX analysis of particle C.	85
Figure 4.9a	(a) SEM micrographs showing particle labelled as D in alloy B4 and (b) EDX analysis of particle D.	86
Figure 4.9b	(a) SEM micrographs showing particle labelled as E in alloy B4 and (b) EDX analysis of particle E.	86
Figure 4.10a	Polarised micrographs of as-received Cu-containing alloys. The pictures were taken of the top section of the alloys.	89
Figure 4.10b	Polarised micrographs of as received Cu-free alloys. The pictures were taken of the top section of the alloys.	90
Figure 4.11a	Polarised micrographs of as-received Cu-containing alloys (A1 and A4) taken from edge and centre positions along the longitudinal sections.	92
Figure 4.11b	Polarised micrographs of as-received Cu-containing alloys (A1 and A4) taken from edge and centre positions along the transverse sections.	93
Figure 4.12a	Polarised micrographs of as-received Cu-free alloys (B1 and B4) taken from different edge and centre along the longitudinal sections.	94

Figure 4.12b	Polarised micrographs of as-received Cu-free alloys (B1 and B4) taken from different edge and centre along the transverse sections.	95
Figure 4.13a	Optical micrographs of the solution treated Cu-containing alloys. The pictures were taken of the top section of the alloys. (a) unetched and (b) etched alloys.	97
Figure 4.13b	Optical micrographs of the solution treated Cu-free alloys. The pictures were taken of the top section of the alloys. (a) unetched and (b) etched alloys.	98
Figure 4.13b	Continued.	99
Figure 4.14a	Optical micrographs of the solution treated Cu-containing alloys. The pictures were taken from longitudinal section of the alloys. (a) Unetched and (b) Etched.	100
Figure 4.14b	Optical micrographs of the solution treated Cu-free alloys. The pictures were taken from longitudinal section of the alloys. (a) Unetched and (b) Etched.	100
Figure 4.15a	Optical micrographs of the solution treated Cu-containing alloys. The pictures were taken from transverse section of the alloys. (a) Unetched and (b) Etched.	101
Figure 4.15b	Optical micrographs of the solution treated Cu-free alloys. The pictures were taken from transverse section of the alloys. (a) Unetched and (b) Etched.	101
Figure 4.16	(a) SEM micrographs showing particle labelled as P in alloy A4 and (b) EDX analysis of particle P.	102
Figure 4.17	(a) SEM micrographs showing particle labelled as Q in alloy A4 and (b) EDX analysis of particle Q.	103
Figure 4.18	(a) SEM micrographs showing particles labelled as R and S in alloy B4, (b) EDX analysis of particle R and (c) EDX analysis of particle S.	103
Figure 4.19a	(a) TEM micrograph after solution treatment at 530 ^{o}C ± 5 ^{o}C for 5 minutes and then water quenched into cold water showing particles labelled A and B in the alloy A1, (b) EDX spectrum of the particle A in alloy A1 and (c) EDX spectrum of the particle B in alloy A1.	105
Figure 4.19b	(a) TEM micrograph after solution treatment at 530 ^{o}C ± 5 ^{o}C for 5 minutes and then water quenched into cold water showing particles labelled A and B in the alloy A2, (b) EDX spectrum of the particle A in alloy A2 and (c) EDX spectrum of the particle B in alloy A2.	105

Figure 4.19c (a) TEM micrograph after solution treatment at 530 ^{o}C ± 5 ^{o}C for 5 minutes and then water quenched into cold water showing particles labelled A and B in the alloy A3, (b) EDX spectrum of the particle A in alloy A3 and (c) EDX spectrum of the particle B in alloy A3. 106

Figure 4.19d (a) TEM micrograph after solution treatment at 530 ^{o}C ± 5 ^{o}C for 5 minutes and then water quenched into cold water showing particles labelled A and B in the alloy A4, (b) EDX spectrum of the particle A in alloy A4, (c) EDX spectrum of the particle B in alloy A4. 106

Figure 4.20a (a) TEM micrograph after solution treatment at 530 ^{o}C ± 5 ^{o}C for 5 minutes and then water quenched into cold water showing particles labelled A and B in the alloy B1, (b) EDX spectrum of the particle A in alloy B1 and (c) EDX spectrum of the particle B in alloy B1. 107

Figure 4.20b (a) TEM micrograph after solution treatment at 530 ^{o}C ± 5 ^{o}C for 5 minutes and then water quenched into cold water showing particles labelled A and B in the alloy B2, (b) EDX spectrum of the particle A in alloy B2 and (c) EDX spectrum of the particle B in alloy B2. 107

Figure 4.20c (a) TEM micrograph after solution treatment at 530 ^{o}C ± 5 ^{o}C for 5 minutes and then water quenched into cold water showing particles labelled A and B in the alloy B3, (b) EDX spectrum of the particle A in alloy B3 and (c) EDX spectrum of the particle A in alloy B3. 108

Figure 4.20d (a) TEM micrograph after solution treatment at 530 ^{o}C ± 5 ^{o}C for 5 minutes and then water quenched into cold water showing particles labelled A and B in the alloy B4, (b) EDX spectrum of the particle A in alloy B4 and (c) EDX spectrum of the particle B in alloy B4. 108

Figure 4.20e (a) TEM micrograph after solution treatment at 530 ^{o}C ± 5 ^{o}C for 5 minutes and then water quenched into cold water showing particles labelled A and B in the alloy B5, (b) EDX spectrum of the particle A in alloy B5 and (c) EDX spectrum of the particle B in alloy B5. 109

Figure 4.21a Analyses data of TEM-EDX for particles in alloy A1 in solution treatment conditions. 112

Figure 4.21b Analyses data of TEM-EDX for particles in alloy A2 in solution treatment conditions. 113

Figure 4.21c Analyses data of TEM-EDX for particles in alloy A3 in solution treatment conditions. 113

Figure 4.21d Analyses data of TEM-EDX for particles in alloy A4 in solution treatment conditions. 114

Figure 4.22a Analyses data of TEM-EDX for particles in alloy B1 in solution treatment conditions. 114

Figure 4.22b Analyses data of TEM-EDX for particles in alloy B2 in solution treatment conditions. 115

Figure 4.22c Analyses data of TEM-EDX for particles in alloy B3 in solution treatment conditions. 115

Figure 4.22d Analyses data of TEM-EDX for particles in alloy B4 in solution treatment conditions. 116

Figure 4.22e Analyses data of TEM-EDX for particles in alloy B5 in solution treatment conditions. 116

Figure 4.23a Polarised micrograph of solution treated Cu-containing alloys. The pictures were taken from the top section of the alloys. 119

Figure 4.23b Polarised micrograph of solution treated Cu-free alloys. The pictures were taken from the top section of the alloys. 120

Figure 4.24a Polarised micrographs of solution treated Cu-containing alloys (A1 and A4) taken from edge and centre positions along the longitudinal extrusion sections. 122

Figure 4.24b Polarised micrographs of solution treated Cu-free alloys (B1 and B4) taken from edge and centre positions along the longitudinal extrusion sections. 123

Figure 4.25a Micrographs of solution treated Cu-containing alloys (A1 and A4) taken from edge and centre positions along the transverse extrusion sections. 124

Figure 4.25b Micrographs of solution treated Cu-free alloys (B1 and B4) taken from edge and centre positions along the transverse extrusion sections. 125

Figure 4.26a DSC curve of alloy A1 taken at a scan rate of 20 ^{o}C min^{-1}. The sample was scanned immediately after solution treatment at 530 ^{o}C and quenching at 0 ^{o}C. 126

Figure 4.26b DSC curve of alloy A2 taken at a scan rate of 20 ^{o}C min^{-1}. The sample was scanned immediately after solution treatment at 530 ^{o}C and quenching at 0 ^{o}C. 127

Figure 4.26c DSC curve of alloy A3 taken at a scan rate of 20 ^{o}C min^{-1}. The sample was scanned immediately after solution treatment at 530 ^{o}C and quenching at 0 ^{o}C. 127

Figure 4.26d	DSC curve of alloy A4 taken at a scan rate of 20 ^{o}C min^{-1}. The sample was scanned immediately after solution treatment at 530 ^{o}C and quenching at 0 ^{o}C.	128
Figure 4.27a	DSC curve of alloy B1 taken at a scan rate of 20 ^{o}C min^{-1}. The sample was scanned immediately after solution treatment at 530 ^{o}C and quenching at 0 ^{o}C.	128
Figure 4.27b	DSC curve of alloy B2 taken at a scan rate of 20 ^{o}C min^{-1}. The sample was scanned immediately after solution treatment at 530 ^{o}C and quenching at 0 ^{o}C.	129
Figure 4.27c	DSC curve of alloy B3 taken at a scan rate of 20 ^{o}C min^{-1}. The sample was scanned immediately after solution treatment at 530 ^{o}C and quenching at 0 ^{o}C.	129
Figure 4.27d	DSC curve of alloy B4 taken at a scan rate of 20 ^{o}C min^{-1}. The sample was scanned immediately after solution treatment at 530 ^{o}C and quenching at 0 ^{o}C.	130
Figure 4.27e	DSC curve of alloy B5 taken at a scan rate of 20 ^{o}C min^{-1}. The sample was scanned immediately after solution treatment at 530 ^{o}C and quenching at 0 ^{o}C.	130
Figure 4.28	Ageing curves of Cu-containing and Cu-free alloys for ageing at room temperature.	131
Figure 4.29	Ageing curves of Cu-containing alloys for ageing at room temperature.	132
Figure 4.30	Ageing curves of Cu-free alloys for ageing at room temperature.	133
Figure 4.31	Tensile properties of Cu-containing alloys that naturally aged at room temperature for (a) 1 hr, (b) 10 hrs, (c) 100 hrs and (d) 1000 hrs.	135
Figure 4.32	Tensile properties of Cu-free alloys that naturally aged at room temperature for (a) 1 hr, (b) 10 hrs, (c) 100 hrs and (d) 1000 hrs.	137
Figure 4.33	Tensile properties of Cu-containing and Cu-free alloys that naturally aged at room temperature showing the changes in (a) UTS, (b) YS and (c) Elongation with time of ageing.	139
Figure 4.34a	Tensile properties of Cu-containing alloys that naturally aged at room temperature showing the changes in (a) UTS, (b) YS and (c) Elongation with time of ageing.	140

Figure 4.34b	Tensile properties of Cu-free alloys that naturally aged at room temperature showing the changes in (a) UTS, (b) YS and (c) Elongation with time of ageing.	141
Figure 4.35a	Ageing curves of Cu-containing and Cu-free alloys for ageing at 100 ^oC.	142
Figure 4.35b	Ageing curves of Cu-containing and Cu-free alloys for ageing at185 ^oC.	143
Figure 4.35c	Ageing curves of Cu-containing and Cu-free alloys for ageing at 300 ^oC.	143
Figure 4.36a	Ageing curves of Cu-containing alloys for ageing at 100 ^oC.	145
Figure 4.36b	Ageing curves of Cu-containing alloys for ageing at 185 ^oC.	145
Figure 4.36c	Ageing curves of Cu-containing alloys for ageing at 300 ^oC.	146
Figure 4.37a	Ageing curves of Cu-free alloys for ageing at 100 ^oC.	148
Figure 4.37b	Ageing curves of Cu-free alloys for ageing at 185 ^oC.	148
Figure 4.37c	Ageing curves of Cu-free alloys for ageing at 300 ^oC.	149
Figure 4.38a	The effect of ageing time and temperature on hardness of the alloy A1 after ageing at 100, 185 and 300 ^oC.	150
Figure 4.38b	The effect of ageing time and temperature on hardness of the alloy A2 after ageing at 100, 185 and 300 ^oC.	150
Figure 4.38c	The effect of ageing time and temperature on hardness of the alloy A3 after ageing at 100, 185 and 300 ^oC.	151
Figure 4.38d	The effect of ageing time and temperature on hardness of the alloy A4 after ageing at 100, 185 and 300 ^oC.	151
Figure 4.39a	The effect of ageing time and temperature on hardness of the alloy B1 after ageing at 100, 185 and 300 ^oC.	152
Figure 4.39b	The effect of ageing time and temperature on hardness of the alloy B2 after ageing at 100, 185 and 300 ^oC.	152
Figure 4.39c	The effect of ageing time and temperature on hardness of the alloy B3 after ageing at 100, 185 and 300 ^oC.	153
Figure 4.39d	The effect of ageing time and temperature on hardness of the alloy B4 after ageing at 100, 185 and 300 ^oC.	153

Figure 4.39e The effect of ageing time and temperature on hardness of the alloy B5 after ageing at 100, 185 and 300 ^{o}C. 154

Figure 4.40 Tensile properties of Cu containing alloys that artificially aged at 185 ^{o}C for (a) 10 hrs, (b) 30 hrs and (c) 100 hrs. 158

Figure 4.41 Tensile properties of Cu-free alloys that artificially aged at 185 ^{o}C for (a) 10 hrs, (b) 30 hrs and (c) 100 hrs. 160

Figure 4.42 Tensile properties of Cu-containing and Cu-free alloys that artificially aged at 185 ^{o}C showing the changes in (a) UTS, (b) YS and (c) Elongation with time of ageing. 162

Figure 4.43a Tensile properties of Cu-containing alloys that artificially aged at 185 ^{o}C showing the changes in (a) UTS, (b) YS and (c) Elongation with time of ageing. 163

Figure 4.43b Tensile properties of Cu-free alloys that artificially aged at 185 ^{o}C showing the changes in (a) UTS, (b) YS and (c) Elongation with time of ageing. 164

Figure 4.44a The effect of ageing temperature on the tensile properties of Cu-containing alloys. 166

Figure 4.44b The effect of ageing temperature on the tensile properties of Cu-free alloys. 167

Figure 4.44b Continued. 168

Figure 4.45 TEM micrographs and corresponding SAD pattern of alloys aged at 100 ^{o}C for 1000 hrs. Electron beam is in the [100] matrix direction. (a) A1, (b) B1, (c) A4 and (d) B4. Arrows A and B showing faint streak in SAD patterns of alloys A4 and B4 and it can be clearly seen in the screen of computer. 171

Figure 4.46 TEM micrographs of alloys aged at 185 ^{o}C for 30 hrs. Electron beam is in [100] matrix direction. (a) A1, (b) B1, (c) A4 and (d) B4. At this stage, β'' needle-shaped precipitates (shown by arrows) predominate in all dilute alloys. 172

Figure 4.47 TEM micrographs of alloys (e) A4 and (f) B4 aged at 185 ^{o}C for 30 hrs (higher magnification). Electron beam is in [100] matrix direction. The β'' needle-shaped precipitates (shown by arrows) were clearly observed in the less dilute alloys. 172

Figure 4.48 TEM micrographs and corresponding SAD pattern of alloys (a) A1 and (b) B1 aged at 300 ^{o}C for 3 minutes (under-aged). Electron beam is in [100] matrix direction. 173

Figure 4.49	TEM micrographs of alloys (c) A4 and (d) B4 aged at 300 °C for 3 minutes (under-aged). Electron beam is in [100] matrix direction. At this stage, β'' needle-shaped precipitates (shown by arrows) predominate in less dilute alloys.	173
Figure 4.50	TEM micrographs of alloys aged at 300 °C for 1 hour (close to peak-aged). Electron beam is in the [100] matrix direction. (a) A1, (b) B1, (c) A4 and (d) B4. At this stage, β'' needle-shaped precipitates (shown by arrows) predominate in all dilute alloys.	174
Figure 4.51	TEM micrographs of alloys aged at 300 °C for 1000 hour (over-aged). Electron beam is in the [100] matrix direction. (a) A1, (b) B1, (c) A4 and (d) B4. β' rod-shaped precipitates (shown by arrows) were observed in alloy A4 meanwhile coarse precipitates predominate in other dilute alloys.	175
Figure 4.52	TEM micrographs of alloy A4 after ageing at 300 °C for 1000 hour (an image at lower magnification). Electron beam is in the [100] matrix direction. β' rod-shaped (shown by arrows) and coarse precipitates predominate in alloy A4.	175
Figure 4.53	(a) TEM dark field micrographs of alloy B4 after ageing at 300 °C for 1000 hours and (b) EDX spectrum from precipitate labelled P.	179
Figure 4.54	(a) TEM bright field micrographs of alloy B4 after ageing at 300 °C for 1000 hours and (b) EDX spectrum from coarse precipitate labelled Q.	180
Figure 4.55	(a) TEM bright field micrographs of alloy B4 after ageing at 300 °C for 1000 hours and (b) EDX spectrum from coarse precipitate labelled R.	180
Figure 4.56	(a) TEM bright field micrographs of alloy B4 after ageing at 300 °C for 1000 hours and (b) EDX spectrum from coarse precipitate labelled S.	181
Figure 5.1	The pseudo-binary Al and Mg_2Si phase diagram.	209
Figure B-1	Measurements extracted from fringe micrograph and plot used to calculated foil thickness.	233
Figure B-2	Convergent beam electron diffraction pattern from alloy A4, aged for 1 hour at 300 °C.	233

LIST OF SYMBOLS

σ_y	Yield strength
b	Burger vectors
G	Shear modulus
p	Dislocation density
α	Constant
σ_d	Yield strength due to grain size
d	Mean grain diameter
k	Constant
$\sigma_{s.s}$	Strength due to solute atoms in solid solution
X_f	Atomic fraction of solute
ΔG_b	Bonding energy between the solute and the matrix
ξ	Atomic misfit between the solute and the solvent atom
σ_{or}	Strengthening due to Orowan mechanism
G_f	Activation free energy
R	Molar gas constant
λ	Inter-particle spacing
b	Burger factors
ΔG_{hom}	Free energy change for homogeneous nucleation
ΔG_v	Free energy reduction due to the formation of precipitate of volume V
ΔG_s	Misfit strain energy produced because the volume of precipitate does not fit perfectly into the space originally occupied by the matrix
r	Radius of spherical precipitate / particle
ΔG_γ	Surface free energy
A	Surface area of precipitate
γ	Interfacial energy
V	Volume of precipitate
ΔG^*_{homo}	Activation energy barrier for homogeneous nucleation
r^*	Critical radius of a spherical precipitate
ΔG_{het}	Free energy change for heterogeneous nucleation
ΔG_d	Free energy change released when nucleus forms at a non-equilibrium lattice defect in the matrix

V^*	Volume of critical precipitate
$\gamma_{\alpha\alpha}$	Interfacial energy of the grain boundary
$\gamma_{\alpha\beta}$	Interfacial energy between the precipitate and matrix
V_β	Volume of precipitate
$S(\theta)$	Shape factor
$A_{\alpha\beta}$	Precipitate surface area of α/β interface
$A_{\alpha\alpha}$	Grain boundary surface area
r_c^*	Radius of spherical caps
T	Temperature
ΔG^*	Activation energy barrier to nucleation
ΔG^*_{het}	Activation energy barrier for heterogeneous nucleation
$\bar{r}$	Mean particle radius
r_o	Mean particle radius at time, t = 0
X_e	Equilibrium solubility of very large particles
t	Time
D	Diffusion coefficient
X_r	Concentration of solute in equilibrium with a particle interface of radius r
X_∞	Concentration of solute in equilibrium with a planar interface ($r = \infty$)
V_m	Molar volume of particle
I_A	X-ray intensity of element A
I_B	X-ray intensity of element B
$C_{A(M)}$	Weight fractions of A in matrix
$C_{A(P)}$	Weight fractions of A in precipitate
$C_{B(M)}$	Weight fractions of B in matrix
$C_{B(P)}$	Weight fractions of B in precipitate
L_M	Electron beam path length in the matrix
L_P	Electron beam path length in the precipitate
n_k	Integer corresponding to the 1^{th} fringe
ξ_g	Extinction distance
z	Foil thickness
S_i	Excitation deviation for i^{th} fringe
λ_w	Incident beam wavelength

$\Delta\theta_i$	Double the distance between the central bright fringe and the i^{th} dark fringe
d_{hkl}	hkl inter planar spacing
$2\theta_B$	Distance between the diffracted disk and the transmitted disk

LIST OF ABBREVIATIONS

JMatPro	Java-based materials properties
DSC	Differential scanning calorimetry
TEM	Transmission electron microscopy
SEM	Scanning electron microscopy
EDX	Energy dispersive x-ray diffraction
SADP	Selected area diffraction pattern
SSSS	Super saturated solid solution
GP Zones	Guinier-Preston zones
HRTEM	High resolution transmission electron microscopy
XRD	X-ray diffraction
UTS	Ultimate tensile strength
YS	Yield strength
VHN	Vickers hardness number
FESEM	Field emission scanning electron microscopy
CBED	Convergent beam electron diffraction
UA	Under-aged
PA	Peak-aged
OA	Over-aged

KESAN Mg, Si DAN Cu TERHADAP RESPONS PENUAAN BAGI ALOI ALUMINIUM SIRI 6XXX CAIR

ABSTRAK

Kesan magnesium (Mg), silikon (Si) dan kuprum (Cu) serta rawatan haba terhadap respons penuaan bagi aloi cair boleh-dirawat haba siri 6xxx telah dikaji. Aloi tersebut mengandungi di antara 0.22 dan 0.79 berat% Si dan di antara 0.20 dan 0.51 berat% Mg. Dalam kajian ini, sesetengah aloi mengandungi sebanyak 0.1 berat% Cu manakala di antara 0.0001 hingga 0.0002 berat% Cu pula dianggap sebagai aloi-bebas Cu. Untuk mempelajari kesan komposisi terhadap respons penuaannya, kesemua sampel aloi telah dirawat larutan pada suhu $530 \pm 5\ ^{o}C$ selama 5 minit dan disempuh lindap ke dalam air sejuk pada suhu $0\ ^{o}C$ sebelum dilakukan penuaan semulajadi pada suhu bilik dan tiruan pada suhu ternaik. Kesan penuaan semulajadi dan tiruan ke atas sifat-sifat mekanik diukur melalui ujian kekerasan Vickers dan ujian ketegangan. Perkembangan mikrostruktur yang terbentuk sepanjang penuaan tiruan dilihat dengan menggunakan mikroskop electron transmisi (TEM). Hasil kajian telah menunjukkan terdapat perkaitan antara respons penuaan dan komposisi, kekerasan, kekuatan dan mikrostruktur. Semakin tinggi kandungan Mg_2Si dan lebihan Si di dalam aloi telah menambah nilai kekerasan dan kekuatan tegangan serta menunjukkan respons penuaan yang terkuat. Sedikit penambahan kandungan Cu hanya memberi kesan yang sedikit terhadap peningkatan kekerasan, kekuatan dan respons penuaan sepanjang penuaan tiruan. Tiada kesan atau perubahan yang berlaku terhadap sifat-sifat tersebut pada kes penuaan semula jadi. Hasil dari penuaan ini pada suhu $185\ ^{o}C$, butiran mendakan berbentuk jarum terbentuk manakala pada suhu $300\ ^{o}C$ butiran mendakan berbentuk jarum dan rod dengan paksi utamanya selari dengan arah matrik [100] telah dilihat di dalam TEM. Jumlah ketumpatan pemendakan telah meningkat dengan peningkatan kandungan Mg_2Si dan lebihan Si. Tambahan 0.1 berat% Cu telah menghaluskan pemendakan dan meningkatkan ketumpatan butiran mendakan tersebut. Dengan memanjangkan masa penuaan sehingga 1000 jam pada suhu $300\ ^{o}C$ telah menghasilkan mendakan kasar di dalam kebanyakan aloi terlebih penuaan. Analisis dengan TEM-EDX terhadap mendakan kasar pada aloi Al-0.50wt%Mg-0.76wt%Si menunjukkan mendakan tersebut terdiri daripada Mg_2Si, AlFeSi, α-AlMnSi dan Si telah wujud bersama.

EFFECTS OF Mg, Si AND Cu ON AGEING RESPONSE OF DILUTE 6XXX SERIES ALUMINIUM ALLOYS

ABSTRACT

The effects of magnesium (Mg), silicon (Si) and copper (Cu) on ageing response of heat treatable dilute 6xxx series aluminium alloys have been investigated. The alloys contained between 0.22 to 0.79 wt% Si and 0.20 to 0.51 wt% Mg. In this study, some alloys contained 0.1 wt% Cu and others contained 0.001 to 0.002 wt% Cu which were considered as Cu-free alloys. In order to study the effect of composition on the ageing response, the alloys samples were solution treated at 530 ± 5 ^{o}C for 5 minutes and then water quenched into ice water at 0 ^{o}C before naturally aged at room temperature and artificially aged at elevated temperature. The effects of natural ageing and artificial ageing on the ageing response were investigated using Vickers hardness test and tensile test, respectively. The microstructures of artificially aged alloys were investigated by transmission electron microscopy (TEM). The results showed a correlation between ageing response and composition, hardness, strength and microstructure of the alloys. The higher solute contents of Mg_2Si and Silicon in excess (ExSi) in the alloys produced higher hardness and tensile strength and consequently the strongest ageing response. Addition of small Cu content (0.1 wt%) gave only a slight increase in hardness, strength and ageing response during artificial ageing but not in the case of natural ageing. The TEM results revealed that the precipitates formed during artificial ageing at 185 ^{o}C were needles and at 300 ^{o}C were needles and rods with their major axes parallel to [100] of the matrix direction. The number density of precipitates increased as their solute content of Mg_2Si and ExSi increased. Addition of 0.1 wt% Cu refined the precipitates and increased slightly the number density of precipitates in the dilute alloys. It was found that prolong ageing time for 1000 hours at 300 ^{o}C resulted in the formation of coarse precipitates in the most of over-aged alloys. Analysis by TEM-EDX on coarse precipitates of over-aged alloy of alloy Al-0.50wt%Mg-0.76wt%Si indicates that Mg_2Si, AlFeSi, α-AlMnSi and Si precipitates were coexist in this alloy.

CHAPTER 1

INTRODUCTION

1.1 Aluminium and Its Alloys

Aluminium has been identified as the most common metal on earth and it is the third most abundant element of the earth's crust. The atomic number of an aluminium is 13, with face-centred cubic (FCC) crystal structure and its lattice parameter, a = 0.4041 nm. Aluminium has useful characteristics such as a low density and the specific weight is approximately one third of that of steel (2.7 gcm^{-3} compared to steel 7.9 gcm^{-3}).

Pure aluminium is undesirable in most engineering design because it is very soft and has a comparatively low strength (yield strength: 7-11 MPa). Pure aluminium does not have good casting or mechanical properties. The mechanical and physical properties of pure aluminium can be improved by deliberate additions of alloying elements, heat treatment and mechanical working. The most common alloying elements in aluminium alloys are magnesium (Mg), silicon (Si), copper (Cu), zinc (Zn) and manganese (Mn).

Figure 1.1 shows the markets of aluminium consumption in United State and China in the year 2002 (Hunt, 2004). It can be seen that the Chinese market is more heavily toward building and construction and substantially less toward packaging. However, the market in United State is more toward transportation and packaging. Another prospect demand for aluminium applications is found in the automotive industries (Hunt, 2004).

The useful characteristics of aluminium alloys are high reflectivity, high electrical and thermal conductivity, good machining properties, excellent ductility and malleability and the material is completely recyclable. Aluminium alloys are easy to be shaped and they have a very good resistance to corrosion. The aluminium alloys protect themselves naturally from corrosion by forming instantaneously a very thin coherent oxide film on the surface. This acts as a protective coating and prevents further corrosion attack by the environment. A very good corrosion resistant, surface properties and good weldability are factors that together with a low price make them commercially very attractive (Marioara *et al.*, 2003). The unique combinations of properties provided by aluminium alloys make the variety of applications of the material continues to increase. The largest uses of aluminium alloys are in transportation, containers, packaging, building and construction.

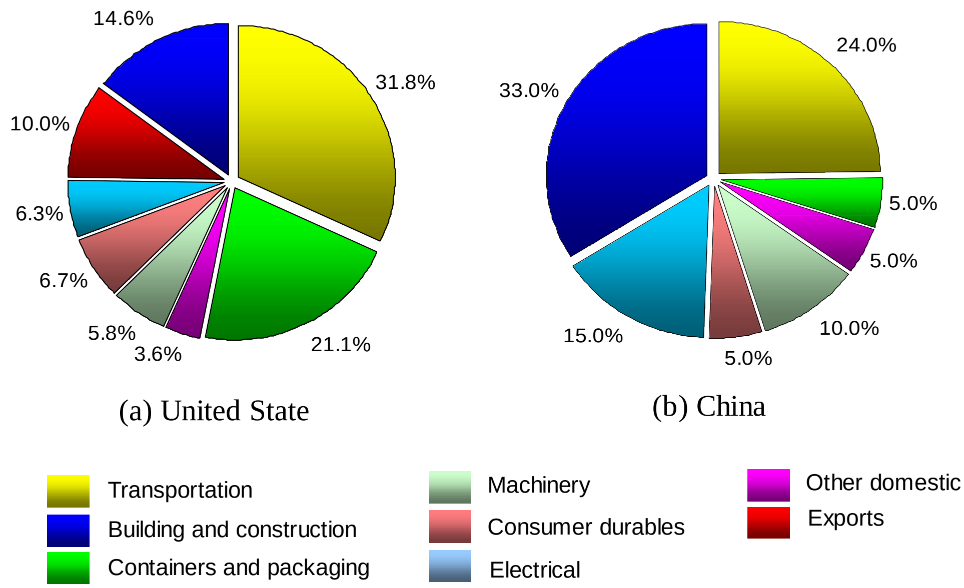

Figure 1.1: The markets of aluminium consumption in United State and China in the year 2002 (Hunt, 2004).

The aluminium alloys can be strengthened by three ways: (i) the elements remain within the aluminium matrix as substitutional solute atoms and strengthening occurs by solid solution strengthening, (ii) the elements dissolved and then precipitated out by suitable heat treatment to form fine precipitates that can give significant strength increase and this is also called precipitation hardening process and (iii) deformation of the alloys during cold working increase the number density of dislocation resulting in modest strength increase.

One of the important types of aluminium alloys is aluminium-magnesium-silicon alloys (Al-Mg-Si) or 6xxx series alloys. Basically they contain Mg and Si as the main alloying elements, but there are significant differences in wt% ratio among them. High strength 6xxx series alloys are characterised by the presence of high content of Mg, Si and Cu. Dilute 6xxx series alloys have been recognised from the low level composition of Mg and Si and other alloying elements. The addition of Mg and Si to aluminium increases the aluminium response to heat treatment due to the formation of Mg_2Si, an intermetallic compound. This improves corrosion resistance as well as the strength of the alloy (Flower, 1995; Gaffar, 2007).

The applications of 6xxx series alloy depend very much on the alloying elements they contain and heat treatments that are given. These alloys have found their greatest use in applications requiring medium to high strength material (Zhen *et al.,* 1997b). Nowadays, the 6xxx series alloys are the most common aluminium alloys that widely used in automotive and aerospace industries, structural applications, engineering sections for building, architecture and construction industries (Ratcliffe, 1993; Ramachandran, 2006; Zuo & Jing, 2008; Abid, 2010). In aluminium related industries, it is very important to enhance the properties of the alloys by applying suitable heat treatment and alteration of alloy composition in order to make them more suitable for fabrication wide range of useful products.

1.2 Problem Statement

Research has focused on 6xxx series alloys since they are being increasingly used in automotive applications such as for panel body car. It is well known that the 6xxx series alloys were chosen due to its ability to form a complex shapes. For car components application, good formability and strength are very important properties that must be focused. It has been found that the paint bake process plays a key role in optimising formability and strength properties (Yassar & Field, 2005). Therefore, the precipitation sequence of the alloys during paint bake process needs to be studied and understood in order to optimise this process.

Although the precipitation hardening process of 6xxx series alloys has been extensively studied by many workers (Miao & Laughlin, 1999 & 2000; Murayama *et al.*, 2001; Yassar & Field, 2005), the understanding of the precipitation hardening process and its sequence is very complex and difficult to optimise since the hardening process is governed by many parameters such as in addition to alloys composition, solution treatment temperature, time between quenching and ageing, ageing time and temperature, which could affect the precipitation hardening behaviours (Miao & Laughlin, 1999; Marioara *et al.*, 2006).

The precipitation hardening process in dilute 6xxx series alloys is still new and not many works has been reported (Aiza *et al.*, 2010)**.** The current study is therefore focused on some dilute 6xxx series alloys and how the heat treatment procedure and their composition can affect the ageing response, microstructure and mechanical properties of the alloys. This alloy has a potential to be used in the automotive industry because it is economical due to less amount of alloying addition used. In this research, hardness measurement, tensile testing and TEM have been used to clarify the complex precipitation hardening processes in 6xxx series dilute alloys.

1.3 Objectives of the Project

The objectives of this work are:

- To investigate the effect of Mg, Si and small addition of Cu on the ageing response during thermal treatment (natural and artificial ageing) of the dilute 6xxx series aluminium alloys.

- To explain the effect of composition on the mechanical properties of the dilute 6xxx series aluminium alloys.

- To study the effect of composition on the microstructural development of some artificially aged dilute 6xxx series aluminium alloys.

- To find out the correlation between the mechanical properties and microstructure of the dilute 6xxx series aluminium alloys.

1.4 Organisation of the Thesis

This thesis consists of six chapters. Chapter 1 introduces the general information on aluminum and its alloys. It is followed by the prospect demand for aluminium application. This chapter also introduces aluminium alloys and the general idea of several ways to strengthen the aluminium alloys. It also briefs the types of 6xxx series alloy and general application of these alloys in various industries including automotive industry.

Chapter 2 provides detail information on designation and the properties of aluminium alloys. This chapter also discusses the topic of heat treatment and strengthening in aluminium alloys. The mechanical properties of aluminium alloys followed by the strengthening mechanism and the effect of precipitates on the strength of alloys are outlined in details. The theory of precipitation hardening and overview of the 6xxx series alloys including the addition to 6xxx series alloys and its applications are also described in this chapter. The end of this chapter explains about precipitation sequences in 6xxx series alloys and reviews the studies by previous researchers chronologically.

Chapter 3 presents the experimental procedure that has been carried out throughout this project. In this chapter, detail information on the materials used that is divided into two groups of alloys i.e Cu-containing and Cu-free alloys are discussed. The details procedure of heat treatment cycle is also discussed in this chapter. This chapter also briefs the JMatPro calculations and Differential Scanning Calorimetry (DSC) procedure. The method of microstructure characterization and mechanical testing (hardness and tensile) are explained. The end of this chapter discusses the TEM procedure and samples preparation.

In chapter 4, the experimental results obtained from Cu-containing and Cu-free 6xxx series alloys are presented. The results are divided into five sections. It begins with studies of JMatPro calculations. The second and third sections are focussed on the characterisation of alloys in the as-received and solution treated conditions. The analyses of some second phase particles using energy dispersive x-ray microanalyses in SEM and TEM-EDX and also extrapolation technique are also presented. The fourth section deals with the results of hardness and tensile of Cu-containing and Cu-free alloys in the naturally aged condition. The fifth section describes the results of hardness and tensile of Cu-containing and Cu-free alloys in artificially aged alloys conditions. The last in this section presents the microstructural developments of artificially aged alloys.

Chapter 5 is the core of this thesis. This chapter discusses the results obtained from investigations of Cu-containing and Cu-free 6xxx series alloys after various heat treatments. The discussion chapter is separated into four sections. Initially, there is explanation on the JMatPro Calculations results. This is followed by the discussion of the alloys characterization results. In sections two and three, the results of as-received and solution treated alloys obtained from the various techniques are compared and discussed. The final section deals with the ageing response. In this section, precipitation and dissolution of the precipitates during DSC heating of as-quenched alloys are explained. Additionally, the effect of the compositions on the ageing response and mechanical properties during natural and artificial ageing are discussed in details. The effect of compositions on the microstructural developments during ageing treatment of the most and less dilute alloys are compared and discussed. Finally, summary of overall results and discussion are presented in the end of this chapter.

Finally, chapter 6 lists the main conclusion remarks of the entire finding found in the results and discussion. Recommendation for future work is proposed in this project.

CHAPTER 2

LITERATURE REVIEW

2.1 Heat Treatment

The principal purpose for the heat treatment is to develop desired mechanical properties required for optimum service performance. The heat-treatment modifies the mechanical properties of the alloys by developing a uniform sub-microscopic structure, thereby increasing the strength and hardness of the alloys. It involves a carefully controlled heating and cooling cycle. The heat treatment is normally based on the following stages (Polmear, 2006):

- Solution treatment: this is where the alloy is held at a relatively high temperature within a single-phase region to bring all alloying elements into solid solution.
- Quenching: this is when the alloy is rapidly cooled from solution treatment temperature to room temperature to obtain a Super Saturated Solid Solution (SSSS) of the elements in the alloy.
- Ageing: age hardening is the process where solute atoms precipitated either at room temperature (natural ageing) or at an elevated temperature (artificial ageing) after quenching.

The age hardenability of alloys is definitely high due to the development of precipitate in the heat treatment. Example of a simplified, pseudo binary phase-diagram of Al-Mg_2Si is shown in Figure 2.1. There are four conditions for an alloy system to have an age-hardening or precipitation hardening response via heat treatment (Askeland, 1984):

- The phase diagram must show a decreasing solid solubility with decreasing temperature.

- The matrix should be relatively soft and ductile but the precipitate should be hard.
- The alloy must be quenchable.
- The precipitates that form must be coherent with the matrix structure in order to develop the maximum strength and hardness.

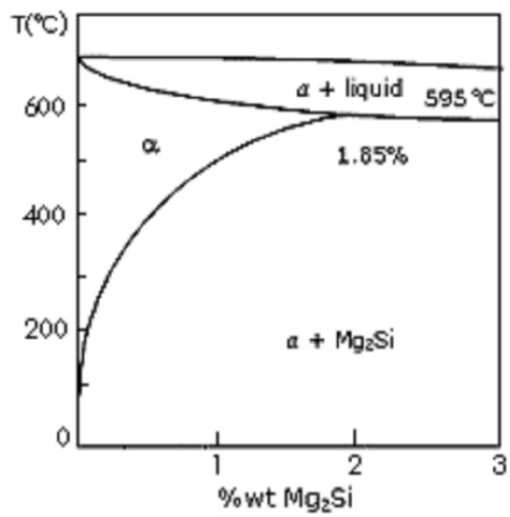

Figure 2.1: The pseudo-binary Al and Mg_2Si phase diagram (Polmear, 2006).

Precipitation hardening provides one of the most widely used mechanisms for the strengthening of metal alloys. There are several general features observed in precipitation hardening reaction (Shewmon, 1969):

- The hardness goes through a broad maximum with time.
- The maximum hardness is reached sooner at higher temperatures.
- The maximum hardness reached decreases as the ageing temperature is increased.
- The fine precipitate of metastable transition phase is initially formed and then it is followed by the formation of equilibrium phase.

The general requirement for precipitation strengthening of supersaturated solid solution (SSSS) involves the formation of finely dispersed precipitates during the ageing. In the case of 6xxx series alloys, the age hardening is used to promote the formation of needle-shaped precipitates (ageing precipitates) from the supersaturated solid solution of Mg and Si in aluminium matrix. The presence of the ageing precipitates can improve the mechanical properties of the alloys.

2.1.1 Solution Treatment

There are two roles of solution treatment: (i) to dissolve precipitates remaining after extrusion or formed during extrusion process and (ii) to relieve stress resulting from the combination of deformation and quenching (Yao *et al.,* 2001). The process consists of heating the aluminium alloys up to an appropriate temperature (between 450 and 550 ^{o}C) and soaking them for a period long enough to achieve a nearly homogeneous solid solution. Time and temperature are important parameters to be controlled during solution treatment.

2.1.2 Quenching

Quenching or cooling is the most critical step in the sequence of heat treatment process. After solution treatment, the alloy rapidly quenched or cooled to room temperature to retain maximum amounts of the alloying elements in solid solution and with minimum precipitates formation. The quenched alloy is a metastable state of supersaturated solid solution. The microstructure formed is thermodynamically unstable and its metallurgical driving force is to move towards the equilibrium structure. In this state, the alloys will have low strength and easy to be formed.

There are two types of cooling: (i) slow cooling (ii) rapid cooling. Slow cooling (e.g air quenching) allows the solute atoms to precipitate out as coarse particles, which reduces the level of supersaturation and hence reducing the effectiveness for the age hardening response. In 6xxx series alloys, slow cooling rates will allow coarse Mg_2Si to precipitate out during the cooling. Therefore, there will be fewer Mg and Si solute atoms to precipitate out during artificial ageing, giving a very small contribution to the strength of the alloys (Reiso, 1984; Birol, 2004).

Rapid cooling (e.g water quenching) will affect the alloys to become stronger as the hardness is increased. Rapid cooling is a fast cooling rate that holds all or nearly all of the solute atoms in solution (Birol, 2004). Since it does not allow sufficient time for solute atoms to precipitate during rapid cooling, therefore, solute atoms in solid solution are available to precipitate out into matrix during ageing. This circumstance produces the maximum ageing response due to high density of ageing precipitates formed.

However, the rapid cooling may leads to residual stresses and cracking. Rapid cooling distorts thinner products and introduces internal (residual) stresses into thicker products (Polmear, 2006). The alloy therefore needs to be aged after quenching to gain the optimum conditions for precipitation during ageing. In this way, the detrimental effects to the mechanical properties and/or corrosion resistance can be avoided.

2.1.3 Ageing

Age hardening is the final stage in the development of properties in the heat-treatable aluminium alloys. The ageing process can be classified into two categories: (a) natural ageing or ageing at room temperature and (b) artificial ageing. These two effects are illustrated diagrammatically in Figure 2.2.

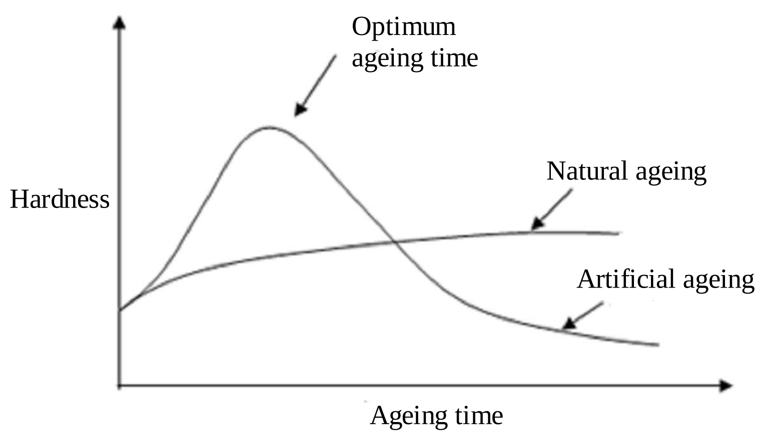

Figure 2.2: Natural and artificial ageing response.

Natural ageing is the process when the precipitation is allowed to complete at room temperature over the necessary period of time. Some aluminium alloys begin the ageing process almost immediately after the alloys are quenched. After a few days, the alloys become considerably stronger. The 6xxx or 7xxx series alloys continue to age hardens over a long period of time at room temperature. For some 7xxx series alloys, this hardening is very marked and typically maximum strength is reached after a month at room temperature (Polmear, 2006).

Many studies have been carried out on the effect of natural ageing on hardness of the 6xxx series alloys. Pashley *et al.*, (1966), Miao & Laughlin (2000), Gupta *et al.*, (2001a) and Cuniberti *et al.*, (2010) reported that the hardening of 6xxx series alloys during natural ageing at room temperature has been related to the formation of very small vacancy-rich cluster and zones. It was found that the formation of Mg and Si clusters increases the hardness of alloys by hindrance of dislocation motion (Muruyama & Hono, 1999). Zhen & Kang (1997), Zhen *et al.*, (1997b), Cabibbo *et al.*, (2003) and Cuniberti *et al.*, (2010) reported that different alloys show different initial hardness level which was dependent upon their amount of solute content present in the alloys. Zhen *et al.*, (1997b) also stated that the longer the natural age, the more clusters are formed and the stability of the clusters increases. Zhen & Kang (1998b) reported that the values of hardness in 6xxx series alloys during natural ageing depend on number density of clusters formed. The number density of clusters is related to the amount of solute atoms of Mg and Si in the matrix. Therefore the higher the Mg and Si content in the alloys, the greater the ageing response and hardness values.

Artificial ageing is the process when precipitation occurs at an elevated or intermediate temperature. It is also called as 'precipitation hardening, 'age hardening' or just 'ageing'. It involves heating the alloy uniformly usually in the range of 160-190 ^{o}C (Polmear, 2006). After solution treatment and artificial ageing, the alloy is stated to be in the T6 temper. Time and temperature of precipitation hardening affect the final structure as well as the resulting mechanical properties. In practice, the ageing time should be long enough to give control of the heat treatment process (Ashby & Jones, 1980).

During ageing at a particular temperature, the mechanical strength of the alloy increases up to a maximum level at a specific ageing time. Beyond this time, the hardness and the strength of the alloy start to decrease. This phenomenon is termed ‘overaging’. It results the particles loosing coherency with the aluminium lattice as they begin to grow larger or coarsen. The larger particles are fewer in number and with greater distances between them. The higher the ageing temperature, the sooner the peak properties are reached and the sooner the overageing begins (Reed-Hill, 1992).

Ageing at much lower temperatures (less than 100 ^oC), longer times are needed to complete the precipitation (Reed-Hill, 1992). Whether the ageing process is performed naturally or artificially, the structure of the alloys goes through similar changes where submiscroscopic precipitates are formed throughout the grain structure. Both natural and artificial ageing results in the decomposition of the SSSS to produce a series of precipitated particles, which may form heterogeneously at preferential sites (e.g. sub-grain boundaries and dislocations) or homogeneously throughout the matrix. The decomposition of the SSSS usually occurs by the following sequence:

$\alpha_{ssss} \rightarrow$ solute atoms clusters or GP zones $\rightarrow$ intermediate precipitate (s)
$\rightarrow$ equilibirium precipitate

Studies by X-ray technique and electron microscopy technique show that the ageing process proceeds initially by the formation of solute atom clusters or Guinier-Preston zones (GP zones). GP zones are ordered, solute-rich cluster of atoms, which may be only one or two atom planes in thickness. They have the same crystal structure as the matrix and fully coherent (Weidmann *et al.*, 1990). The presence of GP zones gives rise to changes in the physical and mechanical properties of the alloys. As they form, the alloy becomes harder.

The diameter of GP zones is about 20 to 40 Å (Shewmon, 1969). The shape of the GP zones dependent on the relative diameters of the solute and solvent atoms. The solutes such as silver and zinc, which have atomic diameters very similar to aluminium, give rise to spherical zones, whereas a solute like Cu, which has a diameter 10% smaller than that of aluminium, forms plate-like zones (Nicholson *et* *al.,* 1958-1959; Martin, 1998). GP zones can act as nucleation sites for other metastable precipitates (Martin & Doherty, 1976).

With prolonged ageing time, the GP zones (clusters) coarsen. The smaller clusters dissolve and their solute atoms join the larger clusters. This decreases the total number of zones and increases the mean diameter of those zones that remain. If the alloy is held at the ageing temperature for a longer time, a new precipitate called intermediate precipitates nucleates and grows. Since the free energy of the alloy can decrease with time, this new precipitate must be more stable than GP zones. The intermediate precipitate(s) are normally much larger than the GP zones; it often makes the alloy harder than when only GP zones are present. The intermediate precipitate has a crystal structure that is different from that of the matrix. It may be partially coherent or coherent with the lattice planes of the matrix in which case a further increase of hardness occurs (Shewmon, 1969; Flower, 1995; Polmear, 2006). The precipitation process will thus continue until the most stable state of precipitate is formed. The final equilibrium precipitates are usually incoherent with the aluminium lattice (Flower, 1995). They normally form at the highest ageing temperatures and their formation produces little hardening because of the coarse dispersion of these precipitates. The formation of the equilibrium incoherent precipitate always leads to softening (Siddiqui & Al-Belushi, 2000; Eivani & Taheri, 2008).

Semi-coherent transition phases nucleate primarily at dislocations and the equilibrium precipitates tend to nucleate and grow at grain boundaries (Martin & Doherty, 1976). All types of precipitates may give hardening but GP zones and intermediate precipitates with some degree of coherency give greater hardening. The presence of GP zones or intermediate precipitates (or both) with their high densities produces the maximum hardening in commercial alloys (Polmear, 2006). They introduce an elastic distortion in the lattice of aluminium matrix and promote a considerable strengthening effect (Anderson *et al.,* 1985; Cabibbo *et al.,* 2003).

The effect of natural ageing is difficult to avoid during common commercial processing in automotive industry (Miao & Laughlin, 2000). For an example in 6xxx series alloys, inferior properties are obtained when some natural ageing is allowed to take place between quenching and artificial ageing (Fortin, 1963; Miao & Laughlin, 1999). During natural ageing, some Mg and Si atoms have been consumed to form clusters therefore the amount of Mg and Si atoms required to form Mg_2Si precipitates during artificial ageing is reduced and this may result in a decrease in final hardness (Miao & Laughlin, 2000).

2.2 Strengthening in Aluminium Alloys

2.2.1 Mechanical Properties of Aluminium Alloys

The precipitation of small particles is important in controlling the microstructure and mechanical properties. Precipitates that form during age hardening have a major effect on the strengthening of aluminium alloys. The main microstructural characteristics that influence the mechanical properties of the alloys are intermetallic compound particles, dispersoid particles and fine precipitates (Flower, 1995). Most of these are explained as follows.

2.2.1.1 Intermetallic Compounds

In aluminium alloys, a different type of intermetallic compound phases is possible to form during cast ingot or billet solidification (Polmear, 2006). The type, size, morphology and distribution of the intermetallic compound particles are very important in determining the subsequent materials properties. The number of the intermetallic compound particles in the final product is determined not only by the casting conditions, but also by subsequent ingot homogenisation and thermomechanical processing (Hsu *et al.*, 2001). The types of intermetallic compound particles that present can be classified into 2 groups: (i) insoluble and (ii) soluble compounds. The size of these particles is greater than 1 μm (Dunwoody *et al.*, 1973; Edward & Martin, 1983). However, Polmear (2006) reported that the size of coarse intermetallic compound within the range of 0.5 to 10 μm.

The first group normally contains impurity elements such as iron (Fe) and Si. The solubility of iron is low in pure aluminium and the degree of its solubility will further decrease with the addition of other alloying elements, so the compound containing iron is insoluble. The brittle and hard intermetallic compound such as α-(Al_8Fe_2Si) and β-(Al_5FeSi) may act as stress raiser and become points of weakness that reduce the strength and ductility of the alloys (Liu *et al.,* 1999). In 7xxx series alloys, the coarse intermetallic compound particles tend to reduce toughness (resistance to crack propagation) but the improvement in these properties can be achieved by reducing the iron impurity content in the alloys (Dunwoody *et al.,* 1973).

The predominant intermetallic compounds in 6xxx series alloys are from the type of AlFeSi (Claves *et al.,* 2002). The AlFeSi phases constitute an important part of the microstructure and they may influence the materials properties during subsequent fabrication steps and play a crucial role for the material quality. The common intermetallic compound particles, exist during the solidification of the 6xxx series alloys are β-(Al_5FeSi). These particles are stable compounds and they are not sensitive to thermal cycles, therefore they are very difficult to dissolve during homogenisation and thus give detrimental effect on mechanical properties of the alloys (Dunwoody *et al.,* 1973; Narayanan *et al.,* 1995; Liu *et al.,* 1999; Claves *et al.,* 2002). Typical other α and β-AlFeSi intermetallics compounds as reported in literature are β-$Al_9Fe_2Si_2$, α-$Al_{12}Fe_3Si_2$, α-Al_8Fe_2Si and α-Al_8FeSi (Liu *et al.,* 1999; Claves *et al.,* 2002; Sha *et al.,* 2006).

In 6xxx series alloys, after casting, irregular bulky shaped of β-AlFeSi phase dominate the microstructure at the grain boundaries and forming an almost continuous network, which reduce the extrusion speed and deteriorate surface quality. During homogenisation process bulky β-AlFeSi phase transform to α-AlFeSi phase, which is shorter, thicker, chunky and round-shaped morphology (Langerweger, 1986; Tanihata *et al.,* 1999; Claves *et al.,* 2002). The α-AlFeSi phase is believed to be less harmful than β-AlFeSi phase form since the presence of this phase is favorable for workability and ductility of the alloys (Kuijpers *et al.,* 2005).

Lamb (1976) reported that the transformation of the β to the α-AlFeSi phase occurred quite rapidly with the presence of Mn but normally the change of shape from bulky β-phase to the more rounded α-phase is less rapid. The initial transformation normally occurs without any shape change and followed by gradual rounding of the particles.

The second group of intermetallic compound particles is soluble compounds that consist of equilibrium intermetallic compounds of the major alloying elements. Examples of the soluble intermetallic compounds are Mg_2Si, Al_2Cu and Al_2CuMg (Polmear, 2006). These compounds form lacy networks around the cast grains. They also can act as sites for crack initiation in the alloys. By homogenisation process, the large intermetallic compound particles can be dissolved and redistributed; therefore the cracking occurs in the alloys can be avoided.

2.2.1.2 Dispersoids

Dispersoids are compounds that are formed during homogenisation of the ingots and they always remain in the microstructure of alloys even after extrusion (Dunwoody *et al.,* 1973; Polmear, 2006). The compounds usually contain the transition elements such as Cr, Mn or Zr, which have a low solubility and diffusivity in aluminium at all temperature. The typical size of dispersoids is within 0.1 to 1 μm (Dunwoody *et al.,* 1973; Martin 1980). Polmear (2006) however, reported that the size of dispersoids varied from 0.05 to 0.5 μm. The transition elements are typically added in small quantities normally less than 1 wt%. Dispersoids are very stable, so they are retained in solution during casting but precipitate during homogenisation which normally occurred at relatively high temperature between 450 to 600 ^{o}C (Dunwoody *et al.,* 1973). Because of low solubility and diffusivity of the dispersoids, they are slow to coarsen and remain as a fine dispersion during processing such as solution treatment and rolling. Examples of dispersoid particles are $Al_{20}Mn_3Cu_2$, $Al_{12}Mg_2Cr$ and Al_3Zr (Polmear, 2006).

The volume fraction of dispersoids is too small to strengthen the alloys directly such as by hindering dislocation motion. Dispersoids occur in different forms depending on the alloying elements and heat treatment conditions. The presence of dispersoids in the alloys gives several effects such as (Dunwoody *et al.,* 1973; Martin, 1980; Livak, 1982; Busby *et al.,* 1986):

- They control grain growth and prevent recrystallization during fabrication, rolling and solution treatment cause increasing in ductility and strength.
- They improve particular properties such as stress-corrosion resistance and toughness.
- The movement of dislocations is impeded and so the end product is harder and stronger.
- They are able to reduce the tendency for intergranular embrittlement in the fully aged condition as well as suppressing the nucleation of fatigue cracks and reducing crack growth.

Dunwoody *et al.,* (1973) studied the effect of incoherent particles on toughness of Al-Mg-Si alloys. They concluded that the toughness of this alloy is increased by the formation of incoherent particles from Fe and Mn elements added. The effectiveness of the particles in promoting toughness is related to their size, where the most effective fine particles size is in the range 0.05 to 0.25 μm**.**

Edward & Martin (1983) investigated the effect of dispersoids on fatigue crack propagation in Al-Mg-Si alloys. It was found that the addition of Mn to the alloy improved resistance to fatigue crack propagation. The decrease in fatique crack growth rate is shown to be a result of a decrease in the degree of intergranular fracture due to the homogenization of slip by the dispersoid particle.

Zhuang *et al*., (1996) reported that Cr and Zr can retard grain growth during recrystallisation. The effectiveness of these elements on the grain refinement is dependent on the volume fraction and size of particles formed during processes before solution treatment. In the alloy with the same concentrations of the dispersoid forming elements, the most effective is Zr, followed by Cr and then Mn.

An investigation by Lodgaard & Ryum (2000), the addition of small amount of Mn and/or Cr has modified the microstructure and improved the properties of the

Al-Mg-Si alloys. Due to high density and thermal stability, dispersoids have a strong effect on the recovery, recrystallisation and grain growth. They also act as nucleation sites for the precipitation of the strengthening precipitates.

2.2.1.3 Fine Precipitates

The precipitates formed during age hardening treatments are usually small in size (less than 0.05 μm) (Blind & Martin, 1983). Polmear (2006) reported that the size of fine precipitates is up to 0.1 μm. This kind of precipitates is a high density of fine coherent and semi-coherent particles that are the major source of strengthening (Dunwoody *et al.,* 1973; Blind & Martin, 1983).

2.2.2 Strengthening Mechanisms

Hindering the motion of dislocations within the material can strengthen commercial alloys. There are several ways to strengthen the metal or alloys such as work hardening (strain hardening), grain size reduction, solid solution strengthening and particle hardening.

2.2.2.1 Work Hardening (Strain Hardening)

Work hardening is a plastic deformation process whereby a ductile metal or alloys becomes harder and stronger (Callister, 1997). During plastic deformation or cold working, the number of dislocations in the alloys increases dramatically due to dislocation multiplication or the formation of new dislocations. This leads to an increase in the yield strength and a decrease in ductility of the material. The increase in yield strength (σ_Y) can be calculated using the relationship:

$$\sigma_y = \sigma_o + \alpha G b \sqrt{p} \qquad (2.1)$$

where σ_o is the yield strength of the matrix, b is Burgers vectors, G is the shear modulus and p is the dislocation density and α is a constant (Callister, 1997).

The increased dislocation density in cold work results in increasing difficulty to dislocations to move through the lattice and cause strengthening effect. Hence, the stress required to deform the material increases with increasing the cold work. However, if the stress required for dislocation motion exceeds that required for crack initiation, the material will fail by cracking.

Dislocation may be removed by heating the cold worked metal or alloys to a moderately high temperature which is called annealing process. This process causes the material to soften and ductility to increase. The changes in the microstructure that occur during annealing are referred to as recovery and recrystallisation.

2.2.2.2 Grain Size Strengthening

Grain size has a very significant influence on the mechanical properties of metal or alloys. This is because neighbouring grains usually have different orientations at the common grain boundary. The hardness of material is observed to increase as the grain size decreases (Verhoeven, 1975). An expression has been developed to describe the relationship between yield strength and the grain size. For many materials, the yield strength varies with grain size, σ_d according to the Hall-Petch equation:

$$\sigma_d = \sigma_o + \frac{k}{\sqrt{d}} \qquad (2.2)$$

where d is the mean grain diameter (m), k is a constant which measures the relative hardening contribution of the grain boundaries and σ_o is the friction stress that must be overcome for dislocations to continue moving. According to the above equation, the grain size should be made as small as possible in order to promote strength of the material.

Grain boundaries act as obstacles to dislocation movement because they interrupt the continuity of the slip planes in a crystal (Newey & Weaver, 1990). During plastic deformation, slip or dislocation motion must take place across the grain boundary. The grain boundary acts as a barrier to dislocation motion for two reasons (Callister, 1997); Firstly, the dislocation will have to change its directions; this becomes more difficult as the misorientation between the grains increases. Secondly, a grain boundary is a localised region of atomic disorder, this may results in a discontinuity of the slip planes from one grain to another and a dislocation cannot pass through it.

Since each grain in a polycrystalline is surrounded by a grain boundary, a dislocation can move only within the grain in which it was created. The more grain boundaries i.e the smaller grain size, the more difficult to plastically deform the material (Newey & Weaver, 1990). This means that a larger applied stress is required to cause slip to pass through a grain boundary in a fine-grained material. Therefore a material with a fine-grained size will be harder and stronger than the same material with a coarse grain size. The fine-grained material will have a greater total grain boundary surface area to stop dislocation movement. It is well known that the grain size reduction improves not only strength but also the toughness of the alloy (Callister, 1997).

2.2.2.3 Solid Solution Strengthening

This form of hardening is present in the early stage of the ageing process. When the solute atoms dissolve in the metal, a solid solution is formed which hardens the metal or alloys. Solid solution strengthening occurs wherever solute atoms are present in the solvent lattice with different atomic size. The presence of solute atoms, since they are of different sizes to the solvents atoms, will distort the crystal lattice; hence they produce a strain field in the lattice.

This mechanism arises from the interactions between strain fields associated with the solute atom and dislocation interaction. The interactions that occur between a dislocation and these distortions (lattice strain field) retard the movement of the dislocation which affects the increase in the shear stress required to move the dislocation. Hence the metal is strengthened.

The magnitude of the solid solution strengthening effect is dependant on the atomic misfit between the solute and the solvent atom (ξ) and the bonding energy between the solute and the matrix (ΔG_b). The increase in strength due to solute atoms in solid solutions ($\sigma_{s.s}$) is given by (Apps, 2001):

$$\sigma_{s.s} = \sigma_o + G\xi\left(\frac{\sqrt{X_f}}{4}\right) + \Delta G_b\sqrt{X_f} \tag{2.3}$$

where σ_o is the yield strength of the matrix, G is the shear modulus and X_f is the atomic fraction of solute. According to the above equation, a large difference of size between the solvent atoms and solutes atom increases the strengthening effect.

The degree of solute solution strengthening also depends on the amount of alloying elements added. The greater the amount of alloying elements added, the greater the strengthening effect. If too much of a large or small atom is added, the solubility limit may be exceeded, thus a dispersion strengthening is produced.

2.2.2.4 Particle Hardening

The hard particles of second phase embedded in the matrix and this lead to resistance to dislocation movement. These particles will interact with the dislocations causing the dislocations to either loop the particles or cut through them. There are three types of particle hardening mechanisms: (i) chemical hardening, (ii) internal strain hardening and (iii) dispersion hardening (Nicholson *et al.*, 1958-1959; Verhoeven, 1975; Smallman, 1985). Details of particle hardening and consequent effects upon strength are dealt with in section 2.2.3.

2.2.3 The Effect of Precipitates on the Strength of Alloys

The strength of an age-hardening alloy is controlled by the interaction of dislocation and precipitates. The strength of the alloys increases as the ageing time increase due to the formation of the precipitates (Eivani & Taheri, 2008). The increase in the strength is dependent on the structure, spacing, size, shape and distribution of the precipitates, the particle-matrix interface and the nature of the dislocations (Hammad *et al.*, 1991).

It is known that GP zones, metastable and stable phases are obstacles to the movement of dislocations. Since the fine precipitates are coherent with the matrix, the dislocations cut or shear through the precipitate as shown in Figure 2.3. This mechanism is produced by chemical hardening or internal strain hardening. The force is required to shear coherent precipitate increases with the number and size of the precipitate. There are three basic processes involved in the cutting mechanism (Peckner, 1964):

- Strengthening by elastic misfit stress. This exists between the precipitate and the matrix since the particles occupy a different volume than the parent phase it replaced.
- Strengthening resulting from the increase in particle surface area due to the cutting and slipping the two halves of the precipitate.
- Strengthening due to shear stress difference, the stress for moving a dislocation inside the precipitate is greater than in the matrix.

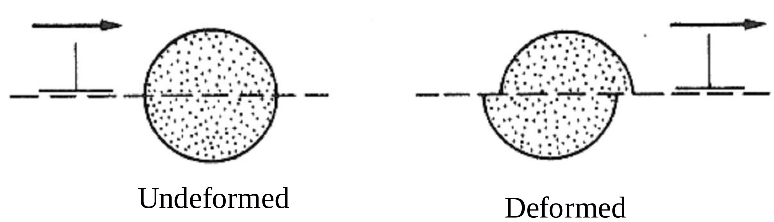

Figure 2.3: Cutting of a fine precipitate by a dislocation (Shewmon, 1969).

The combination of above cutting mechanisms leads to the increase in strength with increasing size and volume fraction of precipitate (Flower, 1995). As ageing time increases, the precipitates will increase in size and slip becomes progressively more difficult. The maximum hardening is generally achieved when the dispersion of precipitates are in the critical size (Smallman, 1985). The effective barrier to dislocation motion causes the resistance to the cutting process. The alloys then reach peak hardness in the optimum ageing time (reasonable time) and the dominant precipitates in this stage are coherent GP zones or intermediate precipitates. The formation of a very fine precipitates is critical in developing a high strength alloy.

For longer ageing time, precipitate coarsening has occurred leading to an increase in precipitate size and inter-precipitate spacing. If precipitate particles are coarse, widely spaced and incoherent with the matrix, the dislocation has difficulty in passing through the material of the precipitate. Thus, dislocations do not cut through precipitates but bend around them, leaving a loop of dislocation as illustrated in Figure 2.4.

.

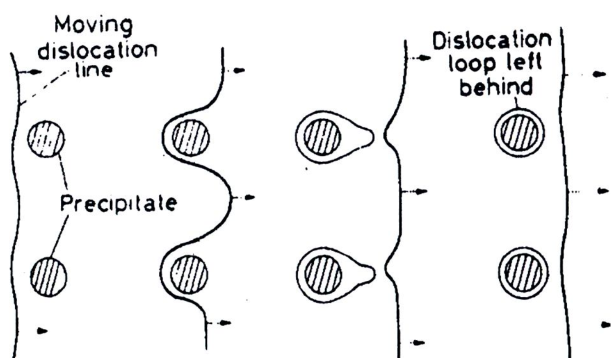

Figure 2.4: Schematic representation of interaction of dislocation with particles (Orowan looping) (Smallman, 1985).

The material's yield stress is inversely proportional to precipitate spacing (Hains, 1977). The yield stress of an alloy will increase as the distance between the precipitates decreases. The more easily dislocation bowing the precipitates making the hardness and yield stress decrease, thus alloys become soften. This circumstance normally occurs when the specimens aged beyond peak hardness, thus it is referred as 'overaged' (Dieter, 1988). The looping mechanism was first proposed by Orowan in 1948 and is referred as the Orowan mechanism (Verhoeven, 1975). The strength due to the hardening given by the Orowan mechanism (σ_{or}) is as below:

$$\sigma_{or} \propto \frac{G_f b}{\lambda} ln \frac{r}{b} \tag{2.4}$$

where G_f is an activation free energy, b is a Burger vector of the dislocation, r is a radius of precipitate and λ is an inter-particle spacing of precipitate (Flower, 1995).

The strengthening due to looping mechanism depends strongly on λ^{-1} and decreases with increasing *r*. This will lead to fewer obstacles to the movement of dislocation and hence the mechanical properties will start to decrease. Orowan bowing is also a process that occurs in hardening dispersion (Smallman, 1985).

The typical age hardening curve is one in which strength increases then decreases with ageing time. This situation is associated by transition from shearing (curve A) to by passing or bowing (curve B) of precipitates. A schematic illustration of the relationship between strength and particle size for a typical age-hardening alloy is given in Figure 2.5. The intersection point P represents the maximum strength, which can be developed in the alloy. Large amount of strengthening can be created by obtaining the microstructure containing precipitates that are resistant to shearing or cutting and are not too widely spaced to allow the bowing of dislocation.

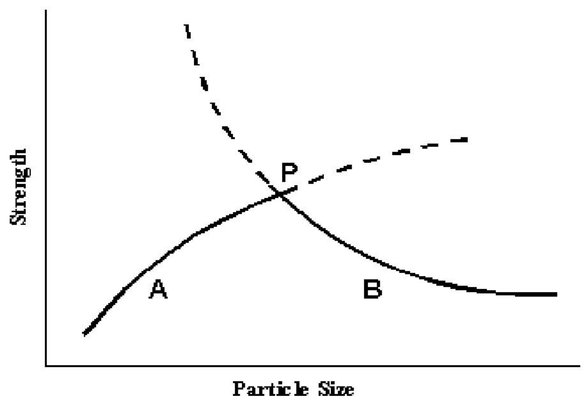

Figure 2.5: Schematic representation of relationship between strength and precipitate particles size for a typical age-hardening alloys: (A) particles sheared or cut by dislocations: (B) particles passed or bowed by dislocation (Polmear, 2006).

2.3 Precipitation Hardening

Precipitation hardening or age hardening provides one of the most widely used mechanisms for the strengthening of aluminium alloys (Meyveci *et al.,* 2010). As mentioned in section 2.2.3**,** the size and shape of the precipitates and the nature of the interface between a precipitate and its matrix have an influence on the mechanical properties of the aged alloys. The influence was determined by the interactions between dislocations and precipitates.